Automotive Experiences
Vol. 6 No. 3 (2023) pp. 515-527
p-ISSN: 2615-6202 e-ISSN: 2615-6636

Research Paper

Coil Spring Failure Analysis Reviewed from Residual Stress, Crytal Orientation, and Texture

Andoko Andoko[1], **Rifqi Ryandi Dwi Ananto**[1], **Heru Suryanto**[1], **Femiana Gapsari**[2], **Maykel Manawan**[3]

[1]Department of Mechanical and Industrial Engineering, Faculty of Engineering, State University of Malang, Malang 65145, Indonesia
[2]Department of Mechanical Engineering, Faculty of Engineering, Brawijaya University, Malang 65145, Indonesia
[3]Department of Physics, Faculty of Military Mathematics and Natural Sciences, Pertahanan University, Bogor 16810, Indonesia

andoko.ft@um.ac.id

https://doi.org/10.31603/ae.9803

Published by Automotive Laboratory of Universitas Muhammadiyah Magelang collaboration with Association of Indonesian Vocational Educators (AIVE)

Article Info
Submitted:
01/08/2023
Revised:
12/11/2023
Accepted:
14/11/2023
Online first:
24/11/2023

Abstract

Crystal defects can be identified through the crystallographic characteristics of crystal orientation (lattice), microstrain and texture. Identification of crystal defects on the atomic scale through crystallography is very important in analyzing the mechanism of material properties due to the influence of dislocations. The slip mechanism is analyzed to minimize coil spring failure. This study aims to analyze the causes of coil spring failure based on crystallography. XRD testing was carried out for analysis of residual stress, crystal orientation, and texture using MAUD 2.94 version software. Hardness testing was carried out on the surface of the coil spring with locations near and far from the fracture using micro vickers. The macro fracture morphology was analyzed using a DSLR camera and the micro fracture morphology was analyzed using SEM. The XRD result show that the coil spring material has a tensile residual stress value of 202.4 ± 15.9 MPa with the resulting crystal orientation showing the *hkl* (100), (200), (211), (200) fields. The plane (200) has a texture characteristic that is oriented towards the Rolling direction along the spring axis. Texture oriented towards Rolling Direction can be shown with a maximum probability value of 1.191. A high probability will have an impact on the presence of material surface defects. Surface defects are indicated by the presence of pits corrosion on micro and macro fracture morphology observations. The pits corrosion defects that occur in the failed coil springs are the beginning of the formation of crack initiation and cause stress concentration. The stress concentration will increase with loading and cause crack propagation.

Keywords: Coil spring; Crystal orientation; Failure analysis; Residual stress; Texture

1. Introduction

Coil springs are generally applied to light vehicles and function under dynamic and static loads [1]. Coil springs are mechanical flexible and absorb energy from the road, while applying force to the suspension to maintain contact between the tire and the road [2]. In the manufacturing process, the coil spring is fabricated by a heat treatment process with a temperature of 950 °C aiming to eliminate stress and maintain elasticity [3]. In the heat treatment process, the material must be at temperature of about 850 °C or often called the austenite temperature [4]. After austenitizing, the spring is quenched whit a certain holding time in an oil tank with a temperature of 80 °C, followed by tempering at a temperature of 400 °C to produce the desired mechanical properties of the coil spring [5]. The coil spring heat treatment process with a temperature that exceeds the critical temperature

can cause decaburation. Decaburation can result in a decrease in fatigue strength and an increase in the rate of crack growth. These conditions can be prevented by an inert atmosphere and recessive warming in the short term [6], [7].

Residual stress can arise after the manufacturing process, and can be in the form of thermal, mechanical, and chemical processes [8]. Residual stress is divided into two types which greatly affect the material properties, including compressive and tensile residual stress [9]–[11]. Compressive residual stress tends to be benefical to the material because it can increase fatigue life. Compressive residual stress improves the size and distribution of surface stress, it results in increased stiffness and decreased vibration amplitude, both of which improve fatigue life [12]–[14]. Tensile residual stress can occur due to non-uniform temperature during the heat treatment process which can lead to crack initiation, this tends to reduce the fatigue life of the material [15]–[17]. The initial failure of the material occurs due to changes in mechanical properties after the fabrication process which can change the direction of stress distribution on the surface of the material [18]. Changes in the direction of stress distribution will affect the intensity of stress concentration which can cause surface defects. The induced stress can be evaluated from the lattice parameters and maximum width (FWHM) using Scherrer line analysis [19]. The analysis can provide a comparison of value of microstrain that occurs which can be assumed as a change in the elastic force between the crystal fields without applying an external load [20].

Various studies on residual stress have attracted the attention of researchers in an effort to increase the fatigue strength of coil springs, the effect of tensile residual stress and relaxation of coil spring tension [21]. The coil spring is subjected to a heat treatment process with time and temperature parameters to eliminate the value of the tensile residual stress. Residual stress was measured on the outer and inner surface of the coil spring to analyze the effect of heat treatment. Heat treatment was carried out, the residual stress value decreased to an interval between 100 and 300 MPa depending on the time and temperature used in the heat treatment. Research on coil springs in nickel-based superalloys at high temperatures has been carried out to analyze stress relaxation and analytical models of torsional creep [22]. The stress relaxation of the the three coil springs was investigated at temperature between 600 °C and 700 °C. Experimental results show that the coil spring relaxes rapidly, decreasing to 50% of the initial force in 1-1000 hours. The stress relaxation increases significantly followed by a change in the value of the dislocation density which can produce persistent residual stress, due to rolling process.

It can be assumed that the poor performance of the coil springs such as decreased fatigue strength is caused by the very high geometric dislocations due to the rolling process. Previous research examined the crack mechanics approach in the cold coiling process with low spring index by combining measurement of residual stress values with neutron analysis and finite element methods [23]. Metallurgical evaluation support was used as evidence to justify the use of the concept of fracture mechanics. The residual stress measurements are then converted into stress intensity factors to allow analysis in fracture mechanics, showing that excessive residual stress caused cracking after the cold coiling process.

Previous research have shown that the residual stress characteristics due to heat treatment and shot peening greatly determine the mechanical properties of the coil spring, especially the fatigue strength [24]–[26]. In addition, other characteristics such as resistance to stress corrosion cracking, and deformation greatly affect the resistance of the coil spring material [27]. Deformation has an important role in observing the texture of the coil spring material [28]. Deformation using the XRD experimental method will produce a preferred crystal orientation which can affect the material properties. Material properties that have low strength occur when the texture pattern of the material is not perfect so that it will create weaknesses in the crystal lattice structure and cause failure [29].

Coil spring on vehicle failed after 191317 *km* of vehicle operation. Based on these problems, an initial analysis of the crystallography of the coil spring failure was determined to be needed. This research aims to identify the causes of coil spring failure through crystallographic observations which include residual stress, crystal orientation, texture, hardness, and fracture morphology.

2. Materials and Method

2.1. Materials

The material used is a coil spring component on the rear suspension of a heavy vehicle, with a fracture in the 2nd coil area out of a total of 6 active coils **Figure 1**. Coil springs samples were produced using hot rolling process based on the specification as described in **Table 1**.

2.2. Chemical Composition Test

The chemical composition of the fractured coil springs was analyzed using a Hilger Emission Spectrometer, Type E-9 OA701, Hilger Analytical, Westwood Margare Kent CT9 4JL, UK. This test is carried out in accordance with ASTM E350 [30].

2.3. Microhardness Test

The micro hardness test aims to analyze the distribution of hardness by making several indentation points on the coil spring material using a micro Vickers hardness tester. (HM-200, Mitutoyo Corparation, Kanagawa 213 8533, Japan). Three indentation points were performed on both specimens near the fracture and far from the fracture **Figure 2**. This test was carried out in accordance ASTM E384 [30].

2.4. Residual Stress, Orientation Crystal, and Texture Test

Residual stress analysis was performed using X-Ray Diffraction (Bruker XRD, Type D8 Advance, Bruker axs GmbH, Kalsruhe, Germany). Experimental was carried out with Cu-Kα1 radiation with a wavelength of 1.5046 [13], [31]. This test is was carried out in accordance with ASTM E2860 [30]. The data results were processed using Qualx 2.1 and Maud 19.2 software.

2.5. Fracture Morphology Test

Morphological observations both macroscopically and microscopically were carried out to analyze the characteristics of the fracture surface (ductile, brittle, fatigue) using a Canon DSLR (Type EOS 1300D, Tokyo Japan). Microscopic observation were carried out using Scanning Electron Microscopy FEI Type Inspect-S50, Field Electron and Ion Company Hillsboro, Oregon, United States) with ASTM STP 827 Standardization [30].

2.6. Simulation FEA

Simulation was carried out to analyze the location of the maximum and ditribution stress in coil spring. The simulation begins with setting the boundary conditions to ensure that the simulation represents the actual conditions. The location of the boundary conditions is shown in **Figure 7a**, which is at both ends of the coil spring, one end for the load and the other end for the fixed support. A load of 2181.5 N was applied which was obtained from the calculation of the maximum load received by the car. The next process is the meshing which is used to dividing

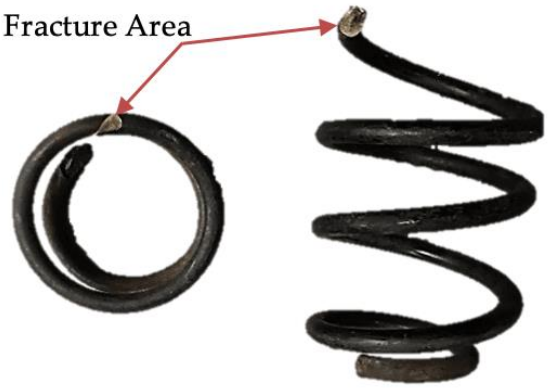

Figure 1. Fracture in coil spring component

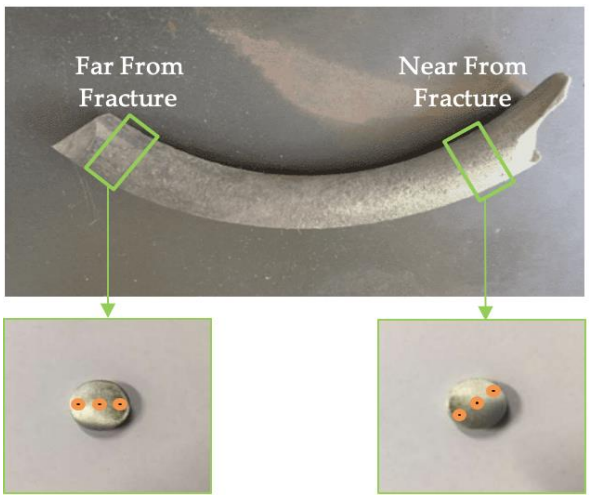

Figure 2. Hardness test indentation

Table 1. Spring specification

Outer Diameter (mm)	Inner Diameter (mm)	Wire Diameter (mm)	Numbers of Total Coils	Free Length (mm)
122	98	12	6 coils 2 passive	350

the model into the smallest parts that aim for a more detailed analysis accuracy, meshing in this analysis uses an element size of 5 mm while at the end of the crack is carried out by the tetrahedron method with a semi-elliptical crack shape at a relatively small ratio of the crack depth above. Solid cylinder diameter (major radius 0.5 mm and minor radius 0.2 mm) which can be seen in **Figure 7b**.

3. Results and Discussion

3.1. Chemical Composition

The chemical composition of the spring material was measured to be C 0.56%, Si 1.6%, Mn 0.78%, P 0.03%, S 0.014%, and Cr 0.65% (**Table 2**). The chemical composition result was compared with the standard spring steels and it was found to be similar to grade SAE 9260 steel. Namely, which is a silicon chromium spring steel that is generally used in the manufacture of coil springs for heavy vehicles. Based on the results of the chemical composition test, the coil springs that failed were included in the medium carbon class category of spring steel. The composition between C, Mn, P, and S is SAE 9260, but the Si element of the coil spring test material does not meet the standard of spring steel. Cr has a high enough value and serves to increase the corrosion resistance of the coil spring.

3.2. Micro Vickers Hardness

Table 3 is the result of micro vickers hardness testing on the coil spring surface. Based on the results of the hardness test, the hardness number of the coil spring exceeds the standardization of raw material grade SAE 9260 (505 HV) [32], [33].

3.3. Residual Stress

The residual stress diffraction pattern was collected in the 2θ range, i.e. 99°-100° with a step size of 0.02°, the slope angle range (ψ) -20° to +20° with a step size of 4° (**Figure 3**). All diffraction patterns were selected to analyze the mean crystal size using the Scherrer relationship, assuming the crystal size is the main source causing the strain effect of the diffraction peaks. There is a difference in the value of FWHM (**Table 4**) at each variation of ψ the angle followed by a large difference in the ratio of crystal sizes. In comparison, the FWHM value is quite large at angle variations of ψ -8°,4°,20° with an average of 3.38 which is almost close to the average value of crystal size.

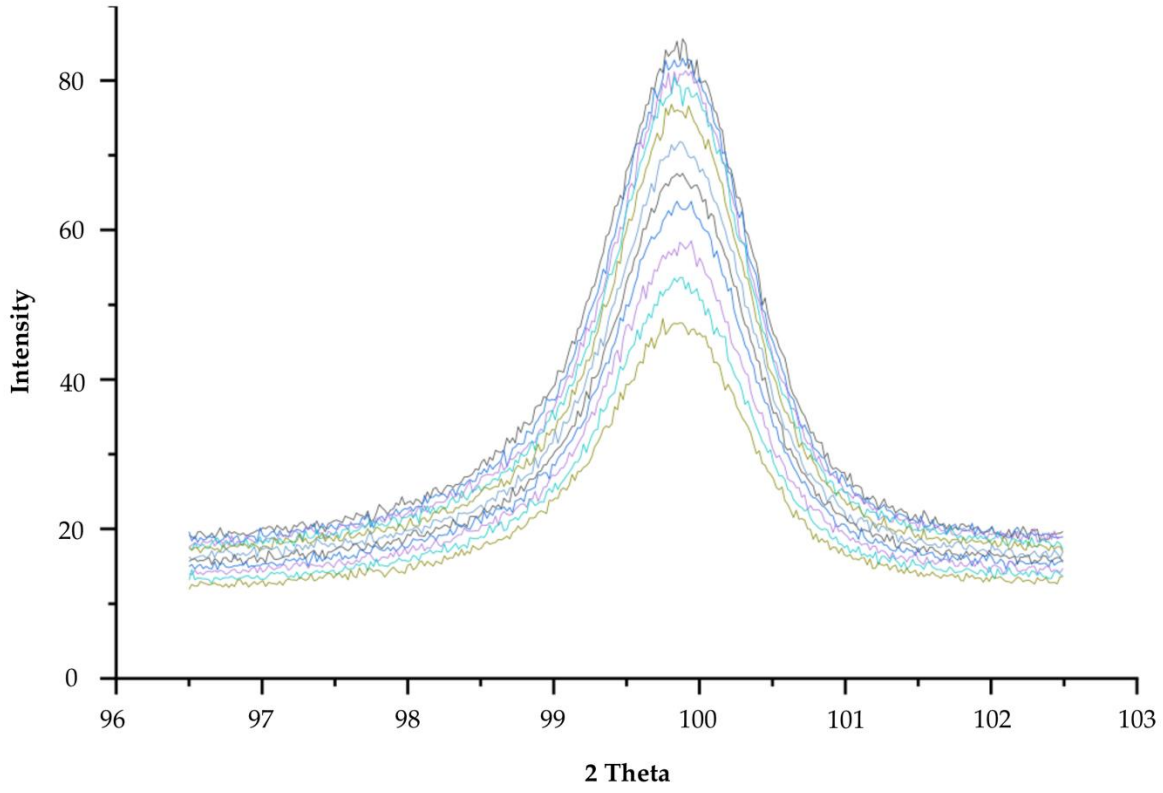

Figure 3. Residual stress diffraction results with ψ angles of -20, -16, -12, -8, -4, 0, 4, 8, 12, 16, 20

Table 2. Chemical composition

Component	C (%)	Si (%)	Mn (%)	P (%)	S (%)	Cr (%)
Coil Spring	0,560	1,601	0,784	0,031	0,014	0,650

Table 3. Vickers hardness number (HV)

Specimen	Indenter Point			Average
	1	2	3	
Near	530.9	577.5	619.2	575.8
Far	502.0	534.3	544.5	526.9

Table 4. FWHM Value of Each Diffraction Pattern

ψ (°)	θ (°)	β (°)	D (μm)	Microstrain
-20	49.880	0.718	3.056	0.151
-16	49.883	0.651	3.375	0.137
-12	49.885	0.715	3.069	0.150
-8	49.886	0.609	3.603	0.128
-4	49.886	0.619	3.545	0.130
0	49.886	0.673	3.261	0.142
4	49.884	0.541	4.056	0.114
8	49.879	0.671	3.271	0.143
12	49.881	0.667	3.291	0.141
16	49.877	0.681	3.221	0.144
20	49.873	0.561	3.917	0.118

Figure 4 shows the tensile stress (negative slope), shear stress (ellipse) and stress gradient (wavy curve) [34]. The highest tensile stress is along the direction of $\sin^2\psi = 0.1$, while the shear stress is present in all directions although its value decreases following the tensile stress path. The undesired tensile stress is 202.4 ±15.9 MPa (30% of the ultimate tensile strength) and the shear stress is 14.3±1.6 MPa (20% of the shear strength in the φ=0° plot.

3.4. Crystal Orientation

The results of the EDS analysis have been carried out on the cracked surface of the coil spring, which detects the Fe phase, so as to obtain the parameter values of d-spacing, crystallite, lattice strain, dislocation (**Table 3**). Then it will get the reflection of the planes (110), (200), (211), and (220) which can be seen in **Table 5**.

Dislocations that occur in the crystal plane can affect the crystal structure due to plastic deformation [28]. The dislocations will form closed loops on the inside of the crystal or on the surface up to a different level of slip along the dislocation line.

3.5. Texture Analysis

The pole figure texture plot is carried out on the coil spring fracture surface with a certain orientation. The pole figure shows the variation of pole density with pole orientation in the (110), (200), and (211) planes (**Figure 6**). The directions of ND, RD and TD on the coil spring sample are shown in **Figure 5**. ND is expressed parallel to the long axis of the coil, RD is perpendicular to the axis and TD is along the coil diameter.

The field (200) shows a comparison of high and low intensity values up to 0.366 compared to the fields (110) and (211). In getting more detailed data from the texture of the component, the image is also needed in the ND (Normal direction), RD (Rolling Direction) and TD (Transverse Direction)

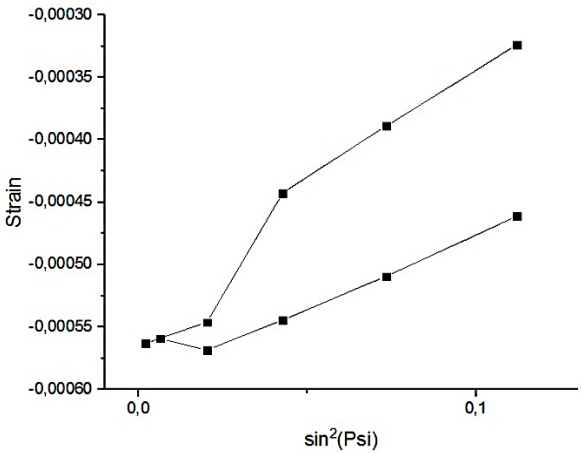

Figure 4. Fundamental equation of X-Ray strain determination

Table 5. Crystal Orientation, Lattice Strain, and Dislocation Parameters

hkl	2θ(°)	d (Å)	D (μm)	E	ϱ
110	52.4	1.74	13.35	5.87	5.6
200	77.3	1.23	8.26	3.61	14.6
211	99.9	1.01	9.78	2.43	10.4
220	124.1	0.87	9.32	1.53	11.5

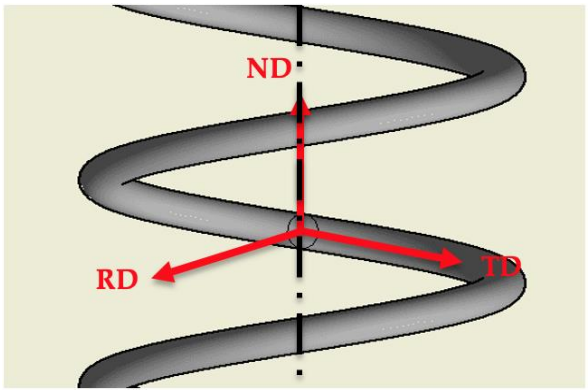

Figure 5. Directions of RD, TD, and ND on the coil spring sample

directions. The ND direction shows that the intensity increases from a random distribution and is concentrated in the (111) plane and tends to experience high texture deformation, while RD and TD have a relatively low density distribution at the poles in the (110) and (100) planes. Plane fibers (111) are frequent slips and distorted dense pile structures intersect in the (110) direction. Therefore screw dislocations can move in these planes, so the slip line is often wavy and difficult to define [35].

3.6. Discussion

The results of the chemical composition that have been discussed previously show that the material of the broken coil spring does not meet the standardization of SAE 9260 material. This condition is indicated by the presence of Si elements which are below the standard. (1.8-2.2%). The element Si in the coil spring material will affect the hardness of the material and affect the solubility of element C in ferrite and the level of stability of cementite [36], [37].

Based on the hardness test on the damaged coil spring, it shows that the highest hardness value is produced at a location close to the fault. The fracture characteristics show that the coil springs fail by fatigue. Fatigue failure is characterized by crack initiation, crack propagation (beachmarks) and final fracture (**Figure 8**). In manufacturing processes such as heat treatment, hot rolling, quenching, to shot peening on coil springs that are not controlled properly will affect the mechanical properties of the material. In manufacturing processes such as heat treatment, hot rolling, quenching, to shot peening on coil springs that are not controlled properly will affect the mechanical

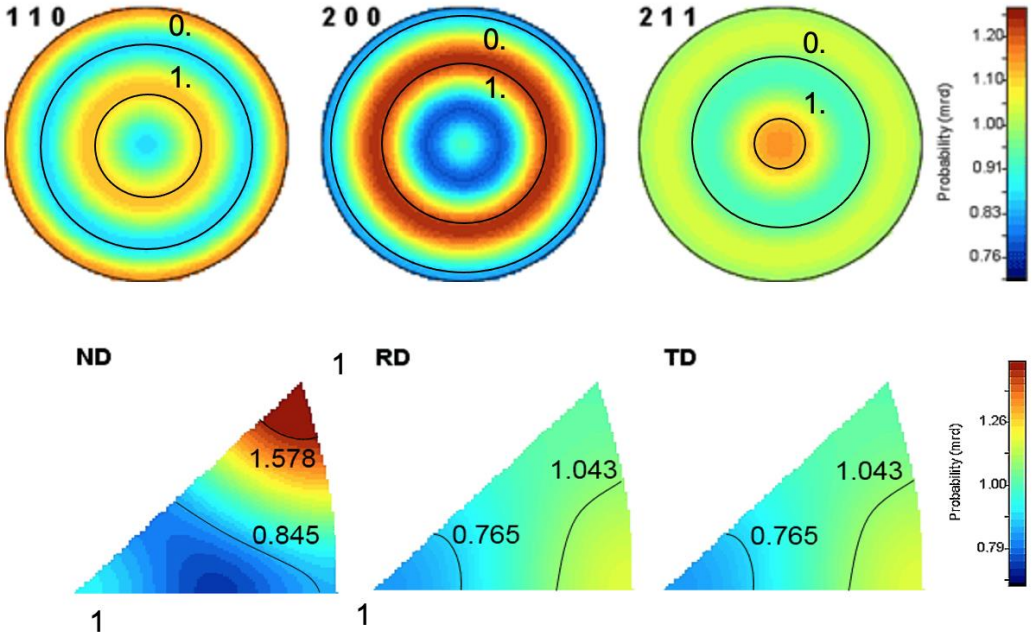

Figure 6. Measurement of pole figure and inverse pole figure on the field (110), (200), and (211)

properties of the material [38]. Especially in hot rolling that is not controlled, it will affect the uniformity of the microstructure value and the residual stress effect given [39], [40]. The hot rolling process requires a temperature of 850 °C, causing the carbon atoms to diffuse from the metal constituent atomic bonds and the formation of the austenite microstructure to produce ductile properties in the material [41]. Austenite will turn to martensite on rapid cooling, but this process has the potential loss that decarburization will reduce ductility and reduce fatigue strength. This will trigger the formation of crack initiation and make stress concentration [4].

The results of X-Ray Diffraction observations were analyzed with Qualx and Maud software to obtain numerical residual stress, crystal orientation, and texture data. There are variations in the increase in FWHM in the residual stress resulting in crystal lattice defects due to the hot rolling process, where the material yields during the first cycle until permanent deformation occurs [42]. This process can lead to the formation of tensile residual stress on the surface of the material [43]. **Figure 3** shows a graph of negative values in accordance with the application of strain resulting in dislocations at the crystal grain boundaries [44]–[46]. The application of non-uniform strain can affect differences in the size of the distortion at the position of the crystal grains, and variations in the distance between planes (hkl), so that the resulting diffraction peaks show differences in peak half plane from the top [47]. The pole figure shows the distribution of the crystallographic direction of the plane (200) selected relative to a value.

The plane (110) is a frequent slip and distorted solid stack structure in the plane (110) intersecting in the 111 direction to show the variation of polar density in the specimen. Texture data can also be presented in the form of inverse pole figures to represent texture fibers. The application of non-uniform strain can affect differences in the size of the distortion at the position of the crystal grains, and variations in the distance between the planes (hkl), so that the resulting diffraction peaks show differences in peak widths [48]. **Table 4** shows that the dislocation density values in the (200) plane are larger with a relatively small ratio of crystal sizes. The greater the value of dislocation density will affect the level of atomic vacancies, which in these conditions allows point defects to occur [49]. The degree of vacancy and the presence of high tensile residual stresses can affect the increase in dislocations causing crack delamination which can accelerate crack propagation due to dynamic loads [50]. In spring steel, there is a significant effect on tensile residual stress during relaxation as the amplitude increases during cyclic loading in the low cycle fatigue limit range [51], [52]. This statement is in accordance with [43] that the results of a study that explained the effect of shot peening on fatigue life and crack mechanisms, especially in low cycle fatigue (LCF) conditions [43], [53]. The presence of tensile residual stress can be controlled by shooting steel balls on the surface of the material (shot peened) to provide compressive residual stress, but the uneven intensity of shot peening tends to produce plastic deformation.

Coil springs experience fatigue fracture that begins with the appearance of pits corrosion due to damage to the surface layer. Pits corrosion then formed crack initiation and propagated to form a beach mark to the final fault in accordance with the results of morphological observations. In the process of operating the coil spring (**Figure 7a**), crack initiation can occur due to the contact between the two coils when holding an overload load (**Figure 7b**) so that it can damage the coating which can trigger early corrosion (**Figure 8a**), so prevention in the way of coating inspection on coil springs is needed to prevent this failure [54]–[56]. Several researchers [23], [54], [57]–[60] have given similar statements regarding the cause of the initiation of crack in coil springs.

Simulations FEA was carried out to strengthen the experimental results based on the value of the crack growth cycle in the material. Coil springs receive dynamic loads that can cause crack growth to reach fracture at a certain (critical) crack length. Mode II has the lowest cyclic value, compared to mode I. In mode II, shearing tends to occur. This can be seen further later on the graph of crack size vs cycle in **Figure 7c**. The cycle value to achieve a critical crack length of 10.28 mm is 97500 cycles . This means that fracture will occur after the crack reaches a length of 10.28 mm or 97500 cycles. When compared with the cycle without cracking, it is seen that the fatigue life with cracks is shorter with the same load. This indicates that cracks play a role in fatigue life. The

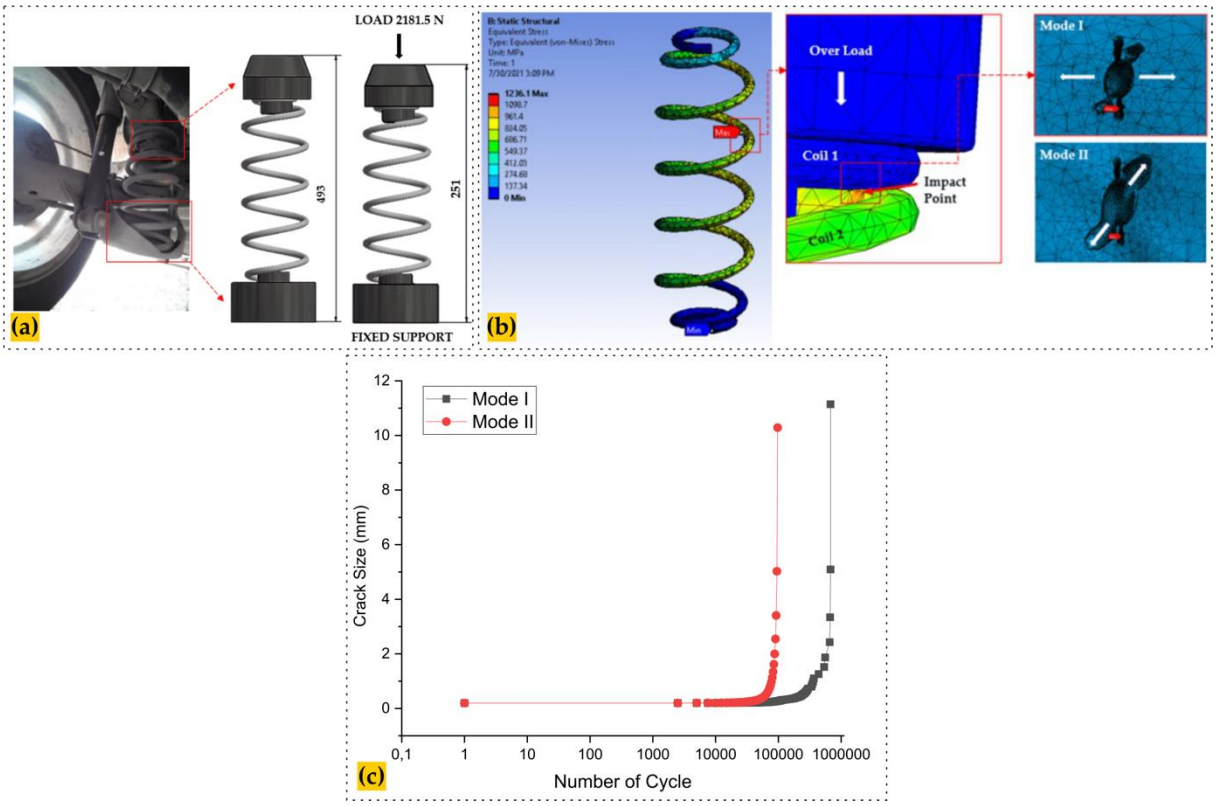

Figure 7. a) Boundary condition, b) Location of collision between coils, c) Graph between crack size vs number of cycle

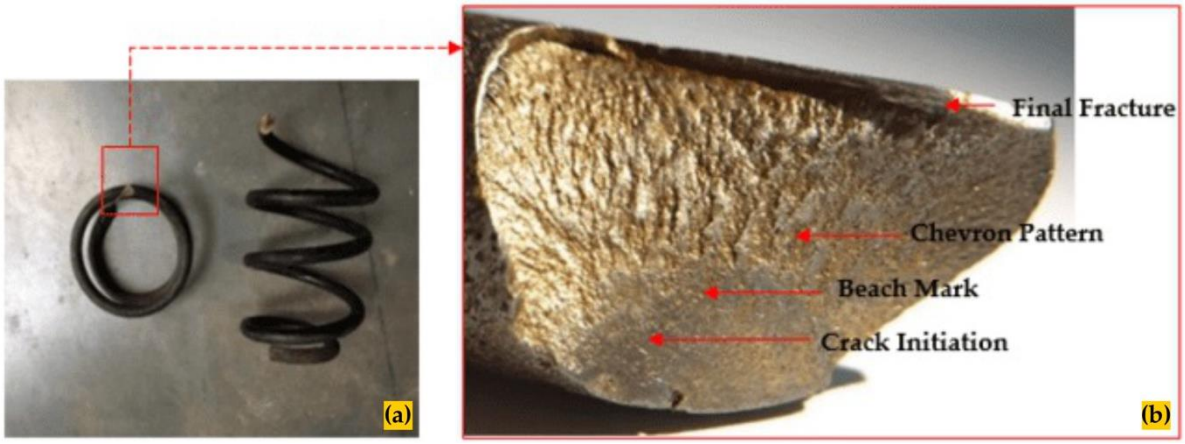

Figure 8. a) Fracture coil spring location, b) Fracture surface

relationship with the failure that occurred was that there was a defect in the coil spring which resulted in a decrease in fatigue life which resulted in a shorter service life compared to normal service life.

These defects can then be characterized through experimental testing. The SEM test was carried out to provide more detailed observations, there were scratches that showed the characteristics of mechanical damage faults (**Figure 9**). Coil spring failure that occurs is included in the fatigue characteristics. Fatigue will have an impact on other corrosion simultaneously, causing the initiation of crack formation. Pits corrosion will be a concentration of stress and damage the protective layer of the coil spring surface (**Figure 10** and **Figure 11**). The crack then propagates to the edge of the surface causing failure of the coil spring shown in **Figure 9** [61]–[63]. Fatigue fracture can be seen by the presence of beachmarks. Beachmarks display a rough and non-uniform surface, this is due to stress concentrations. The stress concentration makes the crack propagation at the beachmarks clearer

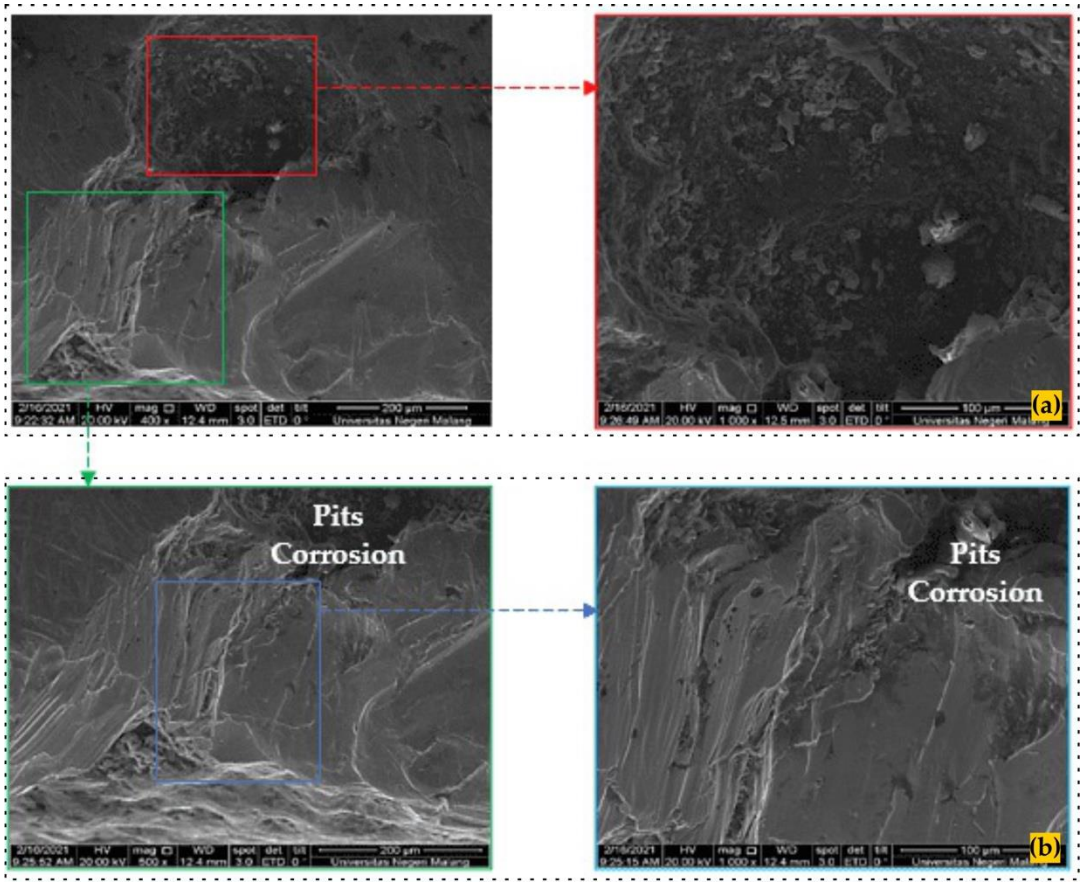

Figure 9. a) Pits corrosion point, b) Fracture damage

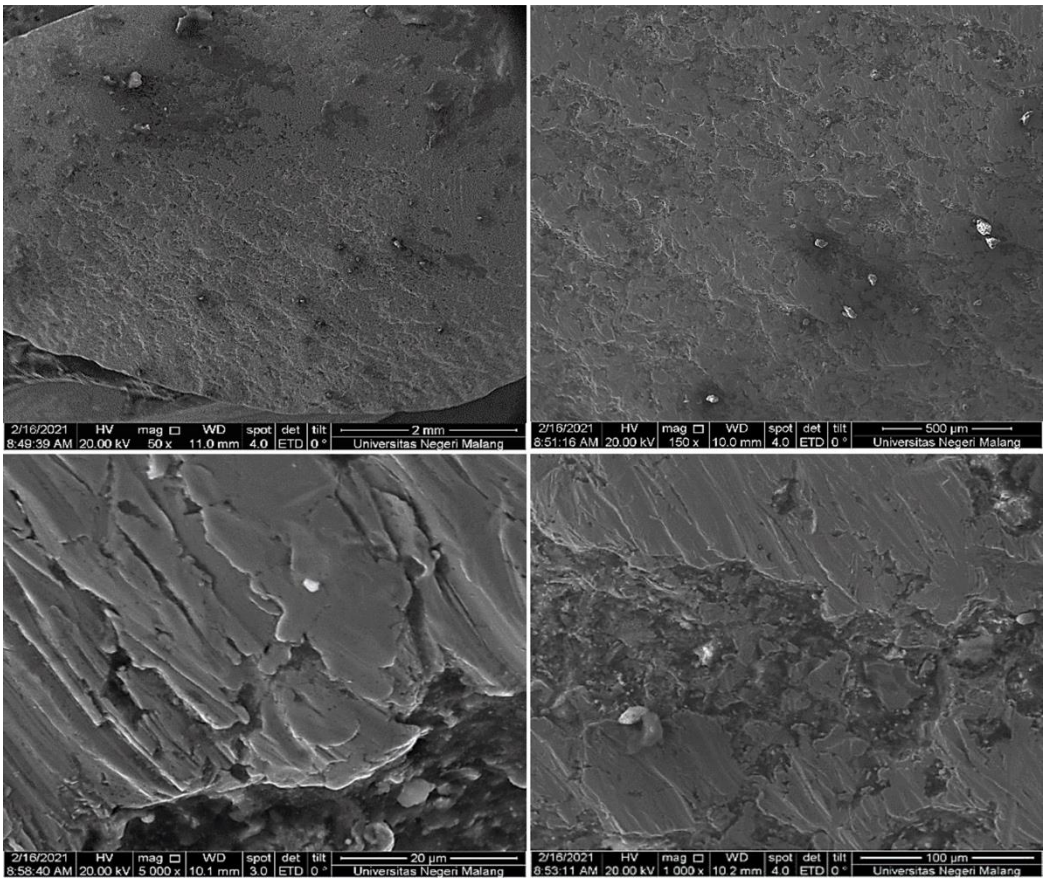

Figure 10. Presence of corrosion

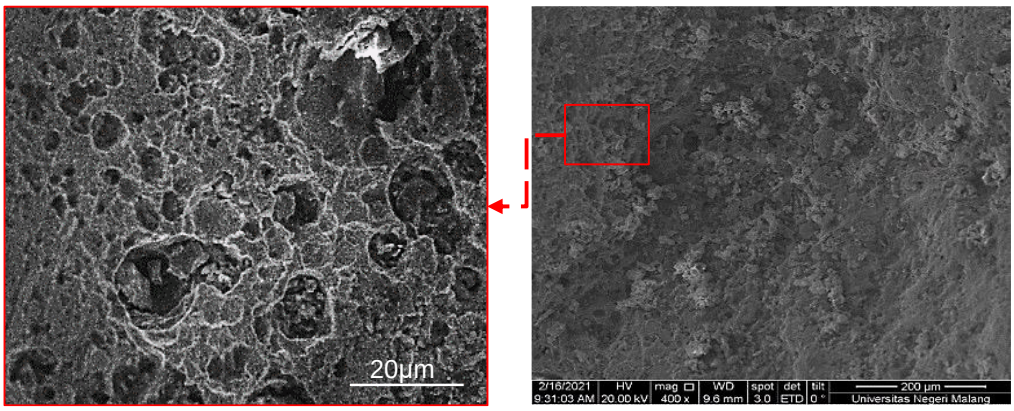

Figure 11. Detail of corrosion

and breaks at higher stress values. These conditions make the consideration that the coil spring has a low cycle fatigue fracture at 200,000 km. Simulationally, the coil spring should be able to last up to the high cycle fatigue region of 3×10^6 cycles [53], [64].

4. Conclusions

In this study, we analyzed the failure of a coil spring. We found that the coil spring failed due to corrosion found at the crack initiation section. The corrosion caused stress concentration indicated by beachmarks. The crack progressed to fracture and was characterized as a fatigue fracture. Another factor contributing to fatigue is the residual stress which is tensile in character, leading to reduced fatigue life. In addition, the dislocation density on the (200) plane is higher which can influence the increase of dislocations leading to crack delamination which can accelerate crack propagation due to dynamic loading. This study shows that corrosion causes coil spring failure and residual stress shortens its fatigue life, so coating and shot peening inspection is needed to prevent this.

Author's Declaration

Authors' contributions and responsibilities

Andoko Andoko: Concept, Analysis, Write; Rifqi Ryandi Dwi Ananto: Experiment, Simulation, Analysis, Write; Heru Suryanto: Analysis, Write; Femiana Gapsari: Analysis, Write; Maykel Manawan: Analysis.

Funding

This research was funding by PNBP UM.

Availability of data and materials

All data are available from the authors.

Competing interests

The authorsdeclare no competing interest.

Additional information

No additional information from the authors.

References

[1] X. Q. Xing, J. N. Lu, J. W. Jian, L. J. Li, and Z. C. Luo, "Effect of environment-assisted cracking on the premature fatigue failure of high-strength valve springs," *Engineering Failure Analysis*, vol. 126, p. 105466, 2021, doi: 10.1016/j.engfailanal.2021.105466.

[2] D. Fakhreddine, T. Mohamed, A. Said, D. Abderrazek, and H. Mohamed, "Finite element method for the stress analysis of isotropic cylindrical helical spring," *European Journal of Mechanics - A/Solids*, vol. 24, no. 6, pp. 1068–1078, 2005, doi: 10.1016/j.euromechsol.2005.07.002.

[3] D. Knowles, *Automotive suspension & steering systems*. Clifton Park, NY: Thomson/Delmar Learning, 2007.

[4] P. M. Kaikkonen, M. C. Somani, I. H. Miettunen, D. A. Porter, S. T. Pallaspuro, and J. I. Kömi, "Constitutive flow behaviour of austenite at low temperatures and its influence on bainite transformation characteristics of ausformed medium-carbon steel," *Materials Science and Engineering: A*, vol. 775, p. 138980, 2020, doi: 10.1016/j.msea.2020.138980.

[5] F. Li, Y. Zhang, H. Wei, and X. Lai, "Integrated problem of soaking pit heating and hot rolling scheduling in steel plants," *Computers & Operations Research*, vol. 108, pp. 238–246, 2019, doi: 10.1016/j.cor.2019.04.016.

[6] H. Soyama, "Comparison between the improvements made to the fatigue strength

of stainless steel by cavitation peening, water jet peening, shot peening and laser peening," *Journal of Materials Processing Technology*, vol. 269, pp. 65–78, 2019, doi: 10.1016/j.jmatprotec.2019.01.030.

[7] H. Soyama and F. Takeo, "Comparison between cavitation peening and shot peening for extending the fatigue life of a duralumin plate with a hole," *Journal of Materials Processing Technology*, vol. 227, pp. 80–87, 2016, doi: 10.1016/j.jmatprotec.2015.08.012.

[8] W. Cheng and I. Finnie, *Residual Stress Measurement and the Slitting Method*. New York: Springer, 2007.

[9] E. Kula and V. Weiss, *Residual Stress and Stress Relaxation*. New York: Springer, 1982.

[10] M. T. Hutchings, *Introduction to the characterization of residual stress by neutron diffraction*. CRC press, 2005.

[11] G. S. Schajer, *Practical residual stress measurement methods*. John Wiley & Sons, 2013.

[12] H. Soyama, T. Kikuchi, M. Nishikawa, and O. Takakuwa, "Introduction of compressive residual stress into stainless steel by employing a cavitating jet in air," *Surface and Coatings Technology*, vol. 205, no. 10, pp. 3167–3174, 2011, doi: 10.1016/j.surfcoat.2010.11.031.

[13] A. Gupta, "Determination of residual stresses for helical compression spring through Debye-Scherrer ring method," *Materials Today: Proceedings*, vol. 25, pp. 654–658, 2020, doi: 10.1016/j.matpr.2019.07.702.

[14] N. Aruchamy, T. Schenk, V. Kovacova, S. Glinsek, E. Defay, and T. Granzow, "Influence of tensile vs. compressive stress on fatigue of lead zirconate titanate thin films," *Journal of the European Ceramic Society*, vol. 41, no. 14, pp. 6991–6999, 2021, doi: 10.1016/j.jeurceramsoc.2021.07.010.

[15] X. Chen, J. Bu, W. Zhou, and Q. Wang, "Effect of pre-cyclic damage and high temperature on residual tensile behavior of concrete," *Fire Safety Journal*, vol. 108, p. 102853, 2019, doi: 10.1016/j.firesaf.2019.102853.

[16] S. Efendi, "Design and Simulation of Cracks in A Four-Cylinder Engine Crankshaft Using Finite Element Method," in *IOP Conference Series: Materials Science and Engineering*, 2019, vol. 494, no. 1, p. 12004, doi: 10.1088/1757-899X/494/1/012004.

[17] H. Liu, S. Hamada, M. Koyama, and H. Noguchi, "Shallow crack effect on evaluation of residual tensile strength: Harmless and stable cracks in finite-sized structure made of ductile metals," *Theoretical and Applied Fracture Mechanics*, vol. 109, p. 102734, 2020, doi: 10.1016/j.tafmec.2020.102734.

[18] S. A. Kumar and N. C. M. Babu, "Influence of induced residual stresses on fatigue performance of cold expanded fastener holes," *Materials Today: Proceedings*, vol. 4, no. 2, pp. 2397–2402, 2017, doi: 10.1016/j.matpr.2017.02.089.

[19] B. D. Cullity and S. R. Stock, *Elements of X-Ray Diffraction*, 3rd in Pea. England: British Library Cataloguing, 2014.

[20] T. R. Gupta, S. S. Sidhu, J. K. Katiyar, and H. S. Payal, "Measurements of lattice strain in cold-rolled CR4 steel sheets using X-ray diffraction," *Materials Science and Engineering: B*, vol. 264, p. 114930, 2021, doi: 10.1016/j.mseb.2020.114930.

[21] L. Del Llano-Vizcaya, C. Rubio-Gonzalez, G. Mesmacque, and A. Banderas-Hernandez, "Stress relief effect on fatigue and relaxation of compression springs," *Materials & design*, vol. 28, no. 4, pp. 1130–1134, 2007, doi: 10.1016/j.matdes.2006.01.033.

[22] S. P. A. Gill, G. McColvin, and A. Strang, "Stress relaxation of nickel-based superalloy helical springs at high temperatures," *Materials Science and Engineering: A*, vol. 613, pp. 117–129, 2014, doi: 10.1016/j.msea.2014.06.080.

[23] Y. Prawoto, S. Manville, T. Sakai, L. Lee, M. Tanaka, and T. Gnaupel-Herold, "Fracture mechanics approach to splitting in low spring index cold coiling process," *Journal of Failure Analysis and Prevention*, vol. 19, pp. 738–751, 2019, doi: 10.1007/s11668-019-00653-7.

[24] D. Čakmak, Z. Tomičević, H. Wolf, Ž. Božić, D. Semenski, and I. Trapić, "Vibration fatigue study of the helical spring in the base-excited inerter-based isolation system," *Engineering Failure Analysis*, vol. 103, pp. 44–56, 2019, doi: 10.1016/j.engfailanal.2019.04.064.

[25] Y. Li, J. Chen, J. Wang, X. Shi, and L. Chen, "Study on the effect of residual stresses on fatigue crack initiation in rails," *International*

Journal of Fatigue, vol. 139, p. 105750, 2020, doi: 10.1016/j.ijfatigue.2020.105750.

[26] V. Martín, J. Vázquez, C. Navarro, and J. Domínguez, "Effect of shot peening residual stresses and surface roughness on fretting fatigue strength of Al 7075-T651," *Tribology International*, vol. 142, p. 106004, 2020, doi: 10.1016/j.triboint.2019.106004.

[27] T. Sigaeva, A. Kolesnikov, and L. Sudak, "Deformation of a closed hyperelastic helical spring," *International Journal of Non-Linear Mechanics*, vol. 110, pp. 1–8, 2019, doi: 10.1016/j.ijnonlinmec.2019.01.005.

[28] M. Shamsujjoha, "Evolution of microstructures, dislocation density and arrangement during deformation of low carbon lath martensitic steels," *Materials Science and Engineering: A*, vol. 776, p. 139039, 2020, doi: 10.1016/j.msea.2020.139039.

[29] A. N. de Moura, C. A. R. Neto, N. A. Castro, E. A. Vieira, and M. T. D. Orlando, "Microstructure, crystallographic texture and strain hardening behavior in hot tensile tests of UNS S32304 Lean Duplex stainless steel," *Journal of Materials Research and Technology*, vol. 12, pp. 1065–1079, 2021, doi: 10.1016/j.jmrt.2021.03.023.

[30] ASTM International, *Mannual book of ASTM standards. Section 13*. West Conshohocken: ASTM International, 2010.

[31] Y. Waseda, E. Matsubara, and K. Shinoda, *X-ray diffraction crystallography: introduction, examples and solved problems*. Springer Science & Business Media, 2011.

[32] S.-K. Kang, Y.-C. Kim, J.-W. Lee, D. Kwon, and J.-Y. Kim, "Effect of contact angle on contact morphology and Vickers hardness measurement in instrumented indentation testing," *International Journal of Mechanical Sciences*, vol. 85, pp. 104–109, 2014, doi: 10.1016/j.ijmecsci.2014.05.002.

[33] P. Ganesh *et al.*, "Studies on fatigue life enhancement of pre-fatigued spring steel specimens using laser shock peening," *Materials & Design (1980-2015)*, vol. 54, pp. 734–741, 2014, doi: 10.1016/j.matdes.2013.08.104.

[34] X. Wang, W. Zhang, J. Ni, T. Zhang, J. Gong, and M. A. Wahab, "Quantitative description between pre-fatigue damage and residual tensile properties of P92 steel," *Materials Science and Engineering: A*, vol. 744, pp. 415–425, 2019, doi: 10.1016/j.msea.2018.12.029.

[35] G. Dini, R. Ueji, A. Najafizadeh, and S. M. Monir-Vaghefi, "Flow stress analysis of TWIP steel via the XRD measurement of dislocation density," *Materials Science and Engineering: A*, vol. 527, no. 10–11, pp. 2759–2763, 2010, doi: 10.1016/j.msea.2010.01.033.

[36] Y. Zhang, H. Sun, H. Wang, X. Wang, X. An, and K. He, "Effects of Cr element on the crystal structure, microstructure, and mechanical properties of FeCrAl alloys," *Materials Science and Engineering: A*, vol. 826, p. 142003, 2021, doi: 10.1016/j.msea.2021.142003.

[37] A. J. McEvily and J. Kasivitamnuay, *Metal failures: mechanisms, analysis, prevention*. John Wiley & Sons, 2013.

[38] M. S. J. Hashmi, *Comprehensive materials processing*. Newnes, 2014.

[39] G. E. Totten, *Handbook of residual stress and deformation of steel*. ASM international, 2002.

[40] Q. Lin, H. Liu, C. Zhu, and R. G. Parker, "Investigation on the effect of shot peening coverage on the surface integrity," *Applied Surface Science*, vol. 489, pp. 66–72, 2019, doi: 10.1016/j.apsusc.2019.05.281.

[41] B. Podgornik, V. Leskovšek, M. Godec, and B. Senčič, "Microstructure refinement and its effect on properties of spring steel," *Materials Science and Engineering: A*, vol. 599, pp. 81–86, 2014, doi: 10.1016/j.msea.2014.01.054.

[42] C. Ha *et al.*, "Texture development and dislocation activities in Mg-Nd and Mg-Ca alloy sheets," *Materials Characterization*, vol. 175, p. 111044, 2021, doi: 10.1016/j.matchar.2021.111044.

[43] R. P. S. Sisodia, M. Gáspár, M. Sepsi, and V. Mertinger, "Dataset on full width at half maximum of residual stress measurement of electron beam welded high strength structural steels (S960QL and S960M) by X-ray diffraction method," *Data in Brief*, vol. 38, p. 107341, 2021, doi: 10.1016/j.dib.2021.107341.

[44] H. Liu *et al.*, "Effect of stress shot peening on the residual stress field and microstructure of nanostructured Mg-8Gd-3Y alloy," *Journal of Materials Research and Technology*, vol. 10, pp. 74–83, 2021, doi: 10.1016/j.jmrt.2020.11.085.

[45] Y. Harada and K. Mori, "Effect of processing

temperature on warm shot peening of spring steel," *Journal of materials processing technology*, vol. 162, pp. 498–503, 2005, doi: 10.1016/j.jmatprotec.2005.02.095.

[46] H.-H. Lai, H.-C. Cheng, C.-Y. Lee, C.-M. Lin, and W. Wu, "Effect of shot peening time on δ/γ residual stress profiles of AISI 304 weld," *Journal of Materials Processing Technology*, vol. 284, p. 116747, 2020, doi: 10.1016/j.jmatprotec.2020.116747.

[47] M. G. Hajiabadi, M. Zamanian, and D. Souri, "Williamson-Hall analysis in evaluation of lattice strain and the density of lattice dislocation for nanometer scaled ZnSe and ZnSe: Cu particles," *Ceramics International*, vol. 45, no. 11, pp. 14084–14089, 2019, doi: 10.1016/j.ceramint.2019.04.107.

[48] R. Li, Q. Tan, Y. Wang, Z. Yan, Z. Ma, and Y.-D. Wang, "Grain-orientation-dependent phase transformation kinetics in austenitic stainless steel under low-temperature uniaxial loading," *Materialia*, vol. 15, p. 101030, 2021, doi: 10.1016/j.mtla.2021.101030.

[49] A. R. Bushroa, R. G. Rahbari, H. H. Masjuki, and M. R. Muhamad, "Approximation of crystallite size and microstrain via XRD line broadening analysis in TiSiN thin films," *Vacuum*, vol. 86, no. 8, pp. 1107–1112, 2012, doi: 10.1016/j.vacuum.2011.10.011.

[50] M. Corrado and J.-F. Molinari, "Effects of residual stresses on the tensile fatigue behavior of concrete," *Cement and Concrete Research*, vol. 89, pp. 206–219, 2016, doi: 10.1016/j.cemconres.2016.08.014.

[51] C. Acevedo and A. Nussbaumer, "Effect of tensile residual stresses on fatigue crack growth and S–N curves in tubular joints loaded in compression," *International Journal of Fatigue*, vol. 36, no. 1, pp. 171–180, 2012, doi: 10.1016/j.ijfatigue.2011.07.013.

[52] M. R. Mitchell, *Residual stress effects on fatigue and fracture testing and incorporation of results into design*, no. 1497. ASTM International, 2007.

[53] S. R. Kumar *et al.*, "Low cycle fatigue behavior of heat treated EN-47 spring steel," *Materials Today: Proceedings*, vol. 22, pp. 2191–2198, 2020, doi: 10.1016/j.matpr.2020.03.299.

[54] D. Pastorcic, G. Vukelic, and Z. Bozic, "Coil spring failure and fatigue analysis," *Engineering Failure Analysis*, vol. 99, pp. 310–318, 2019, doi: 10.1016/j.engfailanal.2019.02.017.

[55] A. Andoko *et al.*, "Simulation of winglet with bend angles of 45, 60 and 90 degree," in *AIP Conference Proceedings*, 2020, vol. 2262, no. 1, doi: 10.1063/5.0015757.

[56] A. Andoko *et al.*, "The influence of crash initiator placement towards the application of energy crash box due to impact load," in *AIP Conference Proceedings*, 2020, vol. 2262, no. 1, doi: 10.1063/5.0015761.

[57] T.-H. Nam, M.-S. Kwon, and J.-G. Kim, "Mechanism of corrosion fatigue cracking of automotive coil spring steel," *Metals and Materials International*, vol. 21, pp. 1023–1030, 2015, doi: 10.1007/s12540-015-5326-5.

[58] G. Vukelic and M. Brcic, "Failure analysis of a motor vehicle coil spring," *Procedia Structural Integrity*, vol. 2, pp. 2944–2950, 2016, doi: 10.1016/j.prostr.2016.06.368.

[59] L. Kosec *et al.*, "Failure analysis of a motor-car coil spring," *Case Studies in Engineering Failure Analysis*, vol. 4, pp. 100–103, 2015, doi: 10.1016/j.csefa.2013.12.004.

[60] F. Bergh, G. C. Silva, C. Silva, and P. Paiva, "Analysis of an automotive coil spring fracture," *Engineering failure analysis*, vol. 129, p. 105679, 2021, doi: 10.1016/j.engfailanal.2021.105679.

[61] A. Andoko *et al.*, "Failure analysis on the connecting rod by finite element method," in *AIP Conference Proceedings*, 2020, vol. 2262, no. 1, doi: 10.1063/5.0015728.

[62] T. L. G. Andoko Andoko, Imam Muda Nauri, Paryono Paryono, Pradhana Kurniawan, Dhanang Reza Pradica, Raymond Philander Jeadi, Riduwan Prasetya, "Failure analysis of connecting rod," *AIP Publishing*, vol. 2262, no. 050013 (2020), 2020, doi: https://doi.org/10.1063/5.0015762.

[63] A. Andoko and P. Puspitasari, "The Fatigue Crack Growth Rate Due to Single-Step Austempered Heat Treatment in Nodular Cast Iron," in *MATEC Web of Conferences*, 2017, vol. 97, doi: 10.1051/matecconf/20179701028.

[64] J. Polak, *Cyclic plasticity and low cycle fatigue life of metals*. Elsevier Amsterdam, 1991.